extraction processes. Oxidation process can limit the reuse of humic acids as fertilizer in agriculture due to the reduction of H/C ratio or nitrogen content. In recent years, membrane technology has become a novel separation technology to purify and clarify effluent water. Several chemical and mechanical treatment processes, such as, chemical coagulation, high speed mechanical stirring and mixing, flocculation, activated sludge treatment electrolysis have been used to treat natural organic matters [11]. The membrane separation processes can offer large number of advantages as compared these conventional methods [12]. This novel separation process is becoming a vital tool for separation of variety of materials ranging from natural organic matter separation to sludge purification. Membrane processes are potentially better for the environmental science since the membrane approach require the use of relatively simple and non-harmful materials. Humic acids substances can be recovered using membrane technology [13]. There are few literatures about the recovery and purification of valuable components like humic acids from paper, food or textile industry waste effluents using membrane ultrafiltration [5].

The aim of this paper is to identify flux decline behavior during humic acids ultrafiltration. The transient flux decline behavior was analyzed at various operating conditions, such as, applied TMP drops and initial feed concentration. The Hermia model was applied to evaluate and confirm the fouling mechanism during dead end ultrafiltration of humic substances. The impact of solute particles and membrane pores to the transient flux decline and permeate quality were studied. The mechanisms of various fouling models were shown using Hermia's model, and the predictions have been matched with experimental values. The fouling behavior of batch cell was also analyzed in terms of variation of total membrane resistance ($R_t$) during operation. Filtration stability and membrane performance were analyzed with respect to volume reduction factor (VRF).

## Materials and Methods

### Materials

Commercial Humic acids powder (HAs), oxidizing agent: potassium dichromate ($K_2Cr_2O_7$), sulphuric acid ($H_2SO_4$), mercuric sulphate ($HgSO_4$), silver sulphate ($Ag_2SO_4$), ferrous ammonium sulphate [$(NH_4)_2$ $Fe(SO_4)_2$ $6H_2O$], cleaning agents: sodium dodecyl sulphate (SDS) and sodium hydroxide (NaOH) were obtained from Loba Chemie, India. All the chemicals were analytical grade and used without further treatment.

### Membrane

The separation process was done using commercial flat sheet asymmetric hydrophilic polyethersulfone membrane, obtained from Permionics Membranes Pvt. Ltd., Vadodara, and Gujarat, India. Molecular weight cutoff was 50 kDa. Membrane characteristics are given in Table 1.

### Experimental setup

**Unstirred batch cell membrane module (U.S.B.C.M.M):** The schematic diagram of unstirred batch cell membrane module (U.S.B.C.M.M) is shown in Figure 1. Air compressor was used to create transmembrane pressure drop during separation through batch cell. A circular polyethersulfone membrane was placed over a metallic support. Rubber gasket was used on the membrane to prevent the leakage. Permeate was collected from the bottom of the batch cell into the measuring cylinder, made by Borosil Glass Works Ltd., Kolkata, India.

### Experimental procedure

In this study, ultrafiltration experiments were conducted using unstirred batch cell membrane module with $33.4 \times 10^{-4}$ $m^2$ membrane area. Batch cell was pressurized with deionized water for 2 hr at 414 kPa applied TMP drop to overcome compaction effect of the fresh membrane. The water flux was measured as a function of time until a steady value was obtained.

### Preparation of synthetic feed sample

Synthetic feed solution was made by dissolving HAs powder sample in Millipore water. Continuous stirring was performed for 1 hr to dissolve the polyfunctional powder sample into the water properly.

### Operating conditions

TMP drop and feed concentration were important parameters during humic acids ultrafiltration. To observe the effects of applied TMP drops, the experiments were carried out by varying operating pressures at 207, 276, 345 and 414 kPa. Feed concentrations were taken as 50, 150 and 250 mg $L^{-1}$. Operating pressure was adjusted with the help air compressor.

### Sample analysis

Solution concentrations were measured using UV-vis spectroscopy (Thermofisher Scientific, India) with $\lambda_{max}$ at 254 nm. The ionic conductivities ($Sm^{-1}$) and total dissolved solids (TDS, mg $L^{-1}$) of all the streams like, feed as well as collected permeates were analyzed by an auto ranging conductivity meter provided by VSI Electronics Pvt. Ltd., Punjab, India. Viscosity was measured using a rheometer at a constant water bath at 28 ± 1°C (HAAKE RheoStress, Thermo Scientific, Germany). pH of the sample was measured by a pH meter provided by Jenway, Bibby Scientific UK. COD was measured on the basis of oxygen consumed during the oxidation of the organic matter in water by a strong oxidizing agent [14].

### Theoretical consideration

Performance of U.S.B.C.M.M. during ultrafiltration of Humic acids at two operating conditions, such as, TMP drop and initial feed concentration were analyzed in terms of permeate flux declination, volume reduction factor (VRF), total membrane resistance ($R_t$).

Permeate flux and membrane hydraulic permeability ($L_p$, $mPa^{-1}s^{-1}$) for UF membrane module with time were analyzed using Darcy's law [15]

$$J_{HAs} = L_P \Delta P = \frac{dV}{A_m dt} = \frac{\Delta P}{\mu R_t} \quad (1)$$

Where $A_m$ the effective membrane area ($m^2$) was, dV was the collected permeate volume (mL). ΔP was TMP drop (kPa). $\mu$ Was the viscosity (Pa s) of permeate sample. $R_t$ Was the total membrane resistance ($m^{-1}$). Total $R_t$ was defined as the combination of three different resistances [15] as:

| Membrane | Unstirred batch cell membrane module |
|---|---|
| Membrane material | Polyethersulfone (PES) |
| Molecular weight cutoff (kDa) | 50 |
| Water permeability at 28°C ($mPa^{-1}s^{-1}$) | $3.974 \times 10^{-11}$ |
| Membrane resistance ( $R_m$, $m^{-1}$) | $1.250 \times 10^{13}$ |
| pH acceptance | 2-14 |
| Maximum temperature tolerance (°C) | 90 |
| Membrane working area ($m^2$) | $33.4 \times 10^{-4}$ |

**Table 1:** Membrane characteristics.

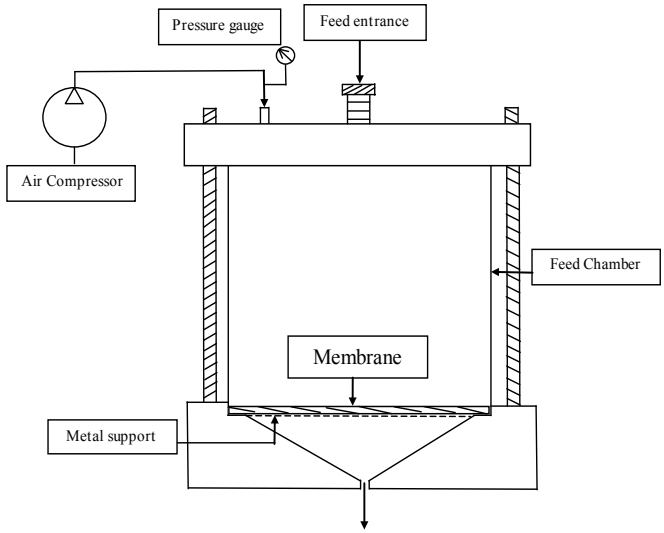


**Figure 1:** Schematic diagram of an unstirred batch cell membrane module (U.B.C.M.M.).

$$R_t = R_c + R_f + R_m \quad (2)$$

$R_c$ Was the cake layer resistance ($m^{-1}$) $R_f$ was the fouling resistance ($m^{-1}$) on membrane surface. $R_{m,}$ fresh membrane resistance before separation was calculated from pure hydraulic flux ($J_w$, $m^3/m^2/min$) using following equation:

$$R_m = \frac{\Delta P}{\mu_w J_w} \quad (3)$$

$\mu_w$ was viscosity (Pa s) of pure water. Fouled membrane resistance ($R_f$ ($m^{-1}$)) was evaluated using following equation:

$$R_f = \frac{\Delta P}{\mu_w J_f} - R_m \quad (4)$$

where $J_f$ ($m^3/m^2/min$) was the calculated water flux after experiment.

Finally, the cake layer resistance can be evaluated using Equation (5)

$$R_c = [R_t - (R_f + R_m)] \quad (5)$$

Variation of observed rejection ($R_{obs}$) defined as under steady state condition

$$R_{obs} = 1 - \frac{C_{p_{HAs}}}{C_{0_{HAs}}} \quad (6)$$

Where $C_{PHAs}$ is solute concentration in the permeate side (mg $L^{-1}$)

$C_{oHAs}$ is solute concentration in the bulk solution (mg $L^{-1}$)

The VRF value was calculated using Equation (7):

$$VRF = \frac{V_0}{V_{R_{HAs}}(t)} = \frac{V_0}{V_0 - V_{P_{HAs}}(t)} \quad (7)$$

where $V_o$ (mL) was the initial feed volume (mL). $V_{RHAS}$ (mL) was the retentate final volume at particular time (t) period. $V_{PHAS}$ (mL) was the collected permeate with respect to time for both modules. VRF values vary from 1 to ∞. At the beginning of operation $V_{R_{HAs}}(t) = V_0$, means VRF = 1. When the entire feed passes through the membrane, $V_{R_{HAs}}(t) = 0$, VRF = ∞ [15,16].

**Analysis of fouling characteristics using hermia model:**

Membrane fouling occurs due to the deposition of retained particles on the membrane surface, pore mouth or pore wall causing transient flux. In the present study, to describe the fouling mechanism, Hermia blocking law model has been used. This law consists of four different fouling models to predict the mode of membrane fouling characteristics, like, complete pore blocking model (CPBM), standard pore blocking model (SPBM), intermediate pore blocking model (IPBM) and cake filtration model (CFM) [17,18]. Figure S1 in the supplementary material illustrates the graphical representation of all types of membrane fouling mechanisms. Equation (8) describes the Hermia blocking model for dead end filtration mode.

$$\frac{d^2t}{dV^2} = K\left(\frac{dt}{dV}\right)^n \quad (8)$$

To analyze each type of fouling module, the parameter n takes different values like,

CPBM $n = 2$, SPBM n=3/2, IPBM $n = 1$, CFM $n = 0$.

Based on the various development of the filtration model, all these four models are linearized in terms of permeate flux with filtration time and are summarized in Table 2.

## Results and Discussion

### Transient flux decline for unstirred batch cell membrane module (U.S.B.M.M.)

Figure 2 shows the variation of permeate flux with time for four TMP drops, such as, 207, 276, 345 and 414 kPa in a dead end unstirred filtration model. As shown in figure, the permeate flux declines sharply with process time for the first 10 mins. Due to the enhancement of driving force, the flux decline increases with increasing TMP drops. For example, it can be observed from Figure 2 that variation of flux decline is maximum at 414 kPa pressure. As the TMP drop increases, the growth of concentration boundary layer on the membrane surface is increased faster due to the faster deposition of rejected solutes [14] This behavior leads to decline the permeate flux at higher pressure drop and gives faster steady flux value. For this reason, the resistance to the water flux decreases with increasing TMP drop producing higher permeates flux. The steady state permeate flux values at different TMP drops of 207, 276, 345 and 414 kPa are 1.82, 2.07, 3.09 and 3.21 × $10^{-4}$ m $min^{-1}$, respectively.

### Effect of feed concentration on permeate flux

Initial feed concentration of pure HAs solution was varied as 50, 150 and 250 mg $L^{-1}$ at constant operating pressure condition (207 kPa). It is clearly seen from Figure 3(a) and 3(b) that, with increasing initial HAs concentration, permeates flux decreases. One interesting behavior has been observed in Figure 3(a) that, with increasing feed concentration from 50 to 150 mg/L, the permeate flux decline is almost same for first 50 mins. At low TMP drop (207 kPa), rejected solute deposition near the membrane surface is slower initially. Due to the dead end filtration, the concentration nearby the membrane surface increases gradually, which gives lower permeate flux at 150 mg $L^{-1}$ than 50 mg $L^{-1}$ after 50 mins of separation. When the feed concentration is 250 mg $L^{-1}$, the permeate flux is lower than other conditions. The high feed concentration can form a gel or cake layer very fast due to the high rejection of solute particles. The gel layer becomes thicker with time which gives lower permeate flux than other initial feed concentrations. When the constant TMP drop is 414 kPa (Refer Figure 3(b)), the permeate flux decreases quickly for each concentration in first 25 mins.

| Different blocking mechanism | Linearized form [18] | | Model Constants (*k*) [18] |
|---|---|---|---|
| CPBM | $\ln J_{HAs} = \ln J_0 - k_c t$ | Membrane pore entrance clogging | $k_c = k_A J_0$ , ($s^{-1}$) |
| SPBM | $\frac{1}{J_{HAs}^{1/2}} = \frac{1}{J_0^{1/2}} + k_s t$ | Deposition of retentate particles over the pore walls | $k_s = 2\frac{k_B}{A_0} A J_0^{1/2}$ , ($m^{-1/2}s^{-1/2}$) |
| IPBM | $\frac{1}{J_{HAs}} = \frac{1}{J_0} + k_i t$ | Pore clogging with membrane surface deposition | $k_i = k_A$ , ($m^{-1}$) |
| CFM | $\frac{1}{J_{HAs}^2} = \frac{1}{J_0^2} + k_{gl_{HAs}} t$ | Membrane surface deposition of the retentate particles | $k_{gl_{HAs}} = \frac{2R_c k_D}{J_0 R_m}$ , ($m^{-2}s^{-2}$) |

**Table 2:** Linearized forms and significances of different blocking mechanisms.

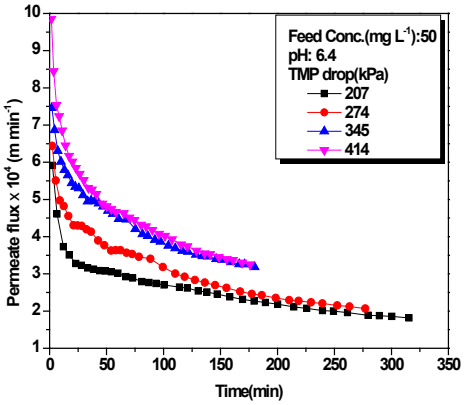


**Figure 2:** Comparison of permeate flux with respect to time at different operating pressures condition during batch cell operation.

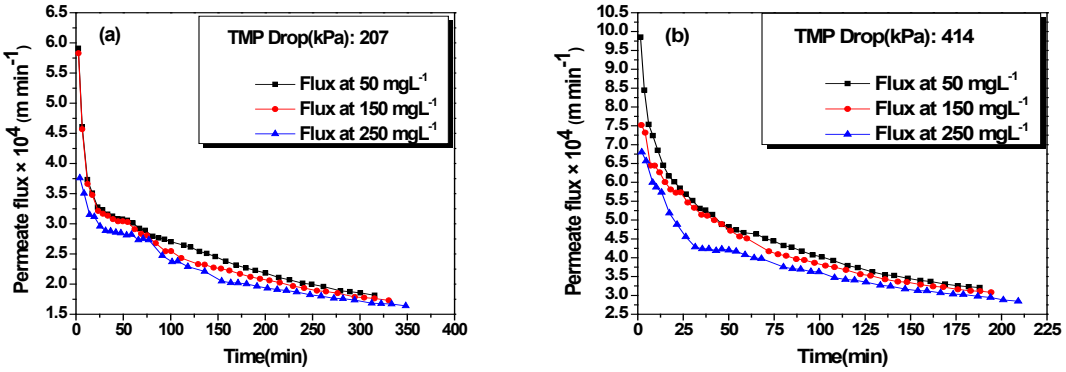


**Figure 3:** Variation of HAs permeate flux at different feed concentration with respect to time at (a) 207 kPa and (b) 414 kPa operating pressure.

This behavior may be assigned to the concentration polarization. HAs particles deposit quickly on the membrane surface and block the active pores in a short time. With gradually increasing feed concentration, membrane fouling assembles into cake formation along with short time. As a result, permeate flux decreases fast with increasing initial feed concentration and reach its steady value faster than lower TPM drop at 207 kPa.

## Variation of observed rejection at different TMP drops during U.S.B.C.M ultrafiltration of HAs solution

Variation of permeate quality in terms of rejection of HAs solutes with TMP drop at three different initial feed concentrations is shown in Figure 4. It is clearly observed that with increasing pressure drop, permeate quality in terms of solute rejection improves for each initial feed concentration. For example, at 50 mg/L feed concentration, an increase in TMP drop from 207 to 414 kPa, solute rejection also increases from 92.1 to 94.2%. For 150 and 250 mg $L^{-1}$, results are 91.5 to 95% and 91.3 to 96%, respectively. This can be described in terms of generation of cake layer due to concentration polarization. At increased TMP drop, rejected solutes form a polarized gel or cake layer which gives additional mass transfer resistance. This resistance acts like a secondary membrane in series with the actual membrane [14]. This interesting phenomenon gives higher rejection at high TMP drop. At constant pressure of 207 kPa with increasing initial feed concentration rejection decreases. This reverse phenomenon has occurred due to the lower compaction of deposited layer which cannot retain the small

particles at high concentration of 150 and 250 mg $L^{-1}$ firstly. As the TMP drop becomes higher, the formed layer also becomes compacted. Thus solutes get obstructed due to the thick layer and give more rejection with increasing initial feed concentration of HAs.

## Variation of VRF with time for U.S.B.C.M operation

Variation of VRF with operating time at different TMP drops (207, 276, 345, 414 kPa) for batch cell operation has been shown in Figure 5. Increase of VRF has a significant impact on membrane permeation. It has an important role over membrane performance as well as permeates quality. With increasing driving force, permeate rate is enhanced resulting VRF to increase. In Figure 5 during batch filtration a sharp change in VRF has been observed. At 207 kPa, VRF value is approx. 3.5. It increases upto 4.5 when pressure drop is 414 kPa within operating time 125 min.

## Application of hermia model

In this present work, Hermia model was used to analyze the fouling characteristics involved in Humic acids dead end ultrafiltration. The more detailed study of this model has been provided to explain the mechanism of pore clogging with different TMP drop conditions. Due to widely distributed molecular weight of the polydispersed materials, elongated morphology and non-rigid chemical structures, some molecules passed through the membrane pores at high TMP drops and caused membrane pore clogging.

Figure 6(a)-(d) shows the implementation of Hermia model to understand the fouling mechanisms, occurring in the humic acids ultrafiltration test. Figure 6(a) shows the fitting of the experimental results to the CPBM. At high TMP drop of 345 and 414 kPa with 50 mg $L^{-1}$ feed concentration, high deviations were obtained between experimental and predicted flux decline. When the size of the rejected solutes is greater than the membrane surface pores, complete pore blocking happens. As a result, solute molecules neither enter into the membrane pores nor arrive to the permeate side.

Figure 6(b) shows the fitting of experimental results to the SPBM. When the size of the solute molecules is lower than of membrane pores, internal blocking occurs due to the solute adsorption onto the membrane pore walls. Figure 6(b) reveals that, solute adsorption was happened partially at low pressure drop. With increasing TMP drop, more amount of solute particles block the pore walls and caused standard blocking.

The theoretical analyses of the experimental permeate flux to IPBM for all parametric conditions have been shown in Figure 6(c). When the membrane pore size is similar to the solute size, membrane pores are blocked just to the entrance of the feed side. When the solutes are not completely retained by the membrane active surface, these molecules can deposit on the others, which were previously deposited. This hypothetic phenomenon occurs in an ultrafiltration process. As a result, IPBM provides a better agreement than SPBM or CPBM to the experimental data.

When the solute sizes are much greater than the membrane pores, a cake layer of retained particles occurs on the membrane surface. This type of phenomena is very common for dead end filtration. With increasing of TMP drop, more solutes are rejected by the membrane pores and create a dense cake layer, causes faster decline of permeate flux. Higher cake compression occurs with higher TMP drops. The thickness of cake layer also depends on increasing of TMP drop and the back transport of molecules towards feed side. Figure 6(d) shows the best fitting of the cake layer formation. The predicted $R^2$ values are very much accurate due to the faster solute deposition on the membrane surface for all the experimental conditions applied during experiment. Table 3 reviews the model constants and initial flux values ($J_0$) for all pore blocking models. It was obtained that the CFB and IPBM revealed the best fitting to flux profile for all the parametric conditions.

## Variation of total resistance during U.S.B.C.M ultrafiltration

Resistance variation with process time is also very important study to check membrane filtration efficiency during separation. During batch cell operation HAs molecules adsorbed on membrane surface resulting in enhanced total resistance. The variation of total resistance with operating time for batch cell operation has been shown in Figure 7. As the TMP drop increases, the growth of concentration boundary layer on the membrane surface is increased rapidly due to the faster deposition of rejected solutes. Hence the total resistance with increasing TMP drop also increases continuously. As shown in Figure 7, total resistance increases from $4.87 \times 10^{13}$ $m^{-1}$ to $7.2 \times 10^{13}$ $m^{-1}$ with increase of TMP drop from 207 to 414 kPa after 2 h operation.

## Permeate quality analysis

Initial HAs concentration in the feed was taken as 50, 150 and 250 mg $L^{-1}$. The COD, pH, ionic conductivity and TDS values are as follows: 165, 450 and 659.2 mg $L^{-1}$; 6.4, 5.4 and 5.03; $2.74 \times 10^{-1}$, $9.4 \times 10^{-1}$ and $5.11 \times 10^{-1}$ S $m^{-1}$; 45, 54 and 60 mg $L^{-1}$, respectively. Table 4 describes the comparison of permeate qualities for different pressure drops in terms of final concentrations, observed rejection (%), ionic conductivity, TDS, pH and final COD values through U.S.B.C.M. It was observed

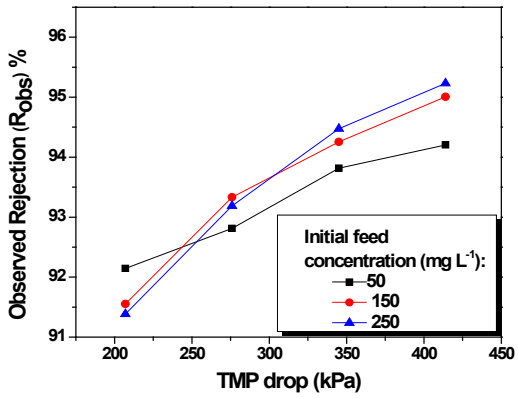


**Figure 4:** Variation of observed rejection with TMP drops.

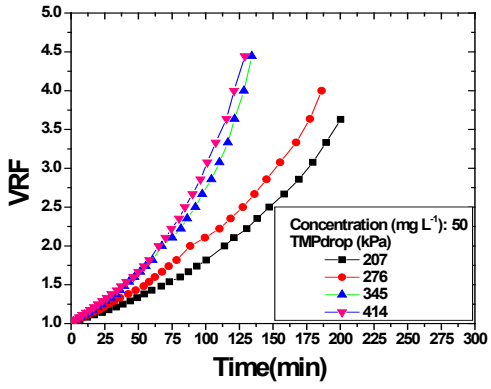


**Figure 5:** Variation of VRF with operating time at different TMP drops during batch cell operation.

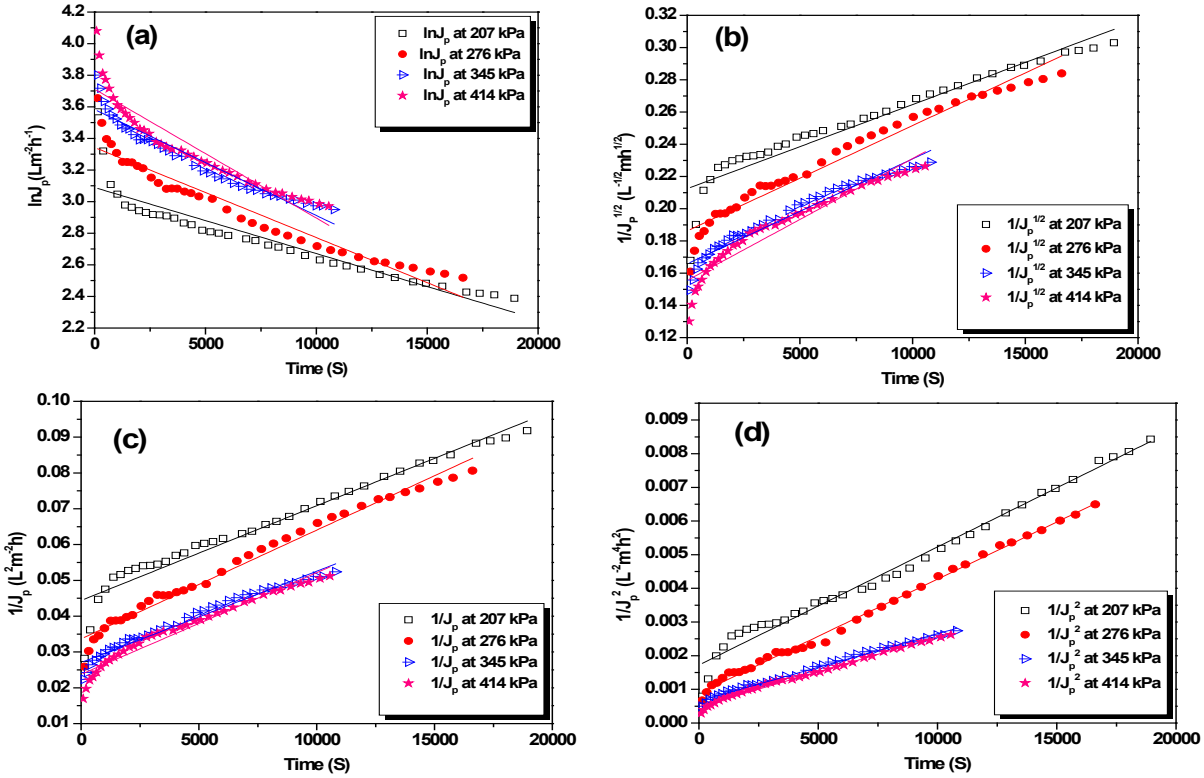


**Figure 6:** Linearized fitness plots for Hermia Pore block models (CPBM (a); SPBM (b); IPBM (c) and CFM (d)) for 50 kDa Membrane cutoff and 50 $mgL^{-1}$ initial feed conditions.

| TMP drop (kPa) | CPBM | | | SPBM | | | IPBM | | | CFM | | |
|---|---|---|---|---|---|---|---|---|---|---|---|---|
| | $k_c \times 10^5$ ($s^{-1}$) | $J_0 \times 10^6$ ($ms^{-1}$) | $R^2$ | $k_s \times 10^6$ ($m^{-1/2}s^{-1/2}$) | $J_0 \times 10^6$ ($ms^{-1}$) | $R^2$ | $k_i \times 10^6$ ($m^{-1}$) | $J_0 \times 10^6$ ($ms^{-1}$) | $R^2$ | $k_{gl_{HAs}} \times 10^7$ ($m^{-2}s$) | $J_0 \times 10^6$ ($ms^{-1}$) | $R^2$ |
| **207** | 4.15 | 7.45 | 0.83 | 5.22 | 6.18 | 0.90 | 2.65 | 6.27 | 0.99 | 3.51 | 7.37 | 0.99 |
| **276** | 5.70 | 8.68 | 0.91 | 6.54 | 8.03 | 0.95 | 3.04 | 7.72 | 0.98 | 3.96 | 9.36 | 0.99 |
| **345** | 6.71 | 11.03 | 0.91 | 6.51 | 10.02 | 0.94 | 2.55 | 10.29 | 0.96 | 4.20 | 10.84 | 0.99 |
| **414** | 8.16 | 12.56 | 0.90 | 7.56 | 11.56 | 0.90 | 2.84 | 11.72 | 0.97 | 4.73 | 20.99 | 0.99 |

**Table 3:** Summary of the model parameters of all pore blocking models for 50 kDa membrane.

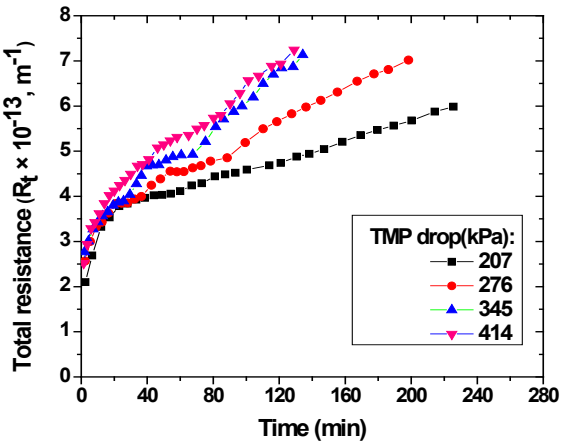


**Figure 7:** Total resistance variation for U.S.B.C.M operation.

| Properties | 50 $mgL^{-1}$ | | | | 150 $mgL^{-1}$ | | | | 250 $mgL^{-1}$ | | | |
|---|---|---|---|---|---|---|---|---|---|---|---|---|
| | ΔP (kPa) | | | | ΔP (kPa) | | | | ΔP (kPa) | | | |
| | 207 | 276 | 345 | 414 | 207 | 276 | 345 | 414 | 207 | 276 | 345 | 414 |
| Permeate conc. ($mgL^{-1}$) | 3.93 | 3.56 | 3.24 | 2.90 | 12.5 | 10.1 | 8.9 | 7.5 | 21.2 | 17.16 | 14.8 | 12.45 |
| Observed rejection (%) | 92.1 | 92.8 | 93.5 | 94.20 | 91.55 | 93.33 | 94.25 | 95 | 91.38 | 93.18 | 94.48 | 95.23 |
| pH | 7.34 | 7.31 | 7.24 | 7.21 | 7.15 | 7.18 | 7.2 | 7.25 | 7.12 | 7.25 | 7.28 | 7.28 |
| Ionic conductivity ($Sm^{-1}$) × $10^{-2}$ | 1.15 | 1.07 | 1.03 | 1.03 | 1.25 | 1.20 | 1.14 | 1.07 | 1.28 | 1.23 | 1.20 | 1.18 |
| TDS ($mgL^{-1}$) × $10^{-3}$ | 6.67 | 6.22 | 6.01 | 5.97 | 7.25 | 6.96 | 6.61 | 6.21 | 7.42 | 7.13 | 6.96 | 6.84 |
| COD ($mgL^{-1}$) | 24.02 | 24.02 | 24.02 | 24.02 | 25 | 25 | 25 | 25 | 28 | 28 | 28 | 28 |

**Table 4:** Physiochemical properties of permeates at steady state during batch cell filtration.

from Table 4 that maximum TDS was removed at 414 kPa. Due to cake layer formation with increased applied pressure, TDS was also removed. Ionic conductivity was decreased from $2.74 \times 10^{-1}$ to $1.15 \times 10^{-2}$ $Sm^{-1}$. With increasing TMP drop, the change in ionic conductivity was marginal for each case. It was found that pH of permeates were changed to 7.25 which become invariant with pressure drops.

## Conclusions

In this study, humic acids water solution was separated through unstirred batch cell module. Applied TMP drops and initial feed concentration were important operating conditions for this system. TMP drop was an important parameter to analyze transient flux declination. Due to high cake layer formation, permeate flux decline was higher at high TMP drop. The nature of the permeate flux was found decreasing with time due to the active pore blocking mechanism during separation. Maximum rejection of 94% was observed at high applied pressure of 414 kPa. With increase in TMP drops, VRF was found to increase exponentially. Hemia pore blocking model was applied to analyze the membrane pore blocking mechanisms. According to the obtained results, it can be determined that the best fits to experimental values are for the CFM and IPBM, for all the TMP drop conditions. In consequence, the values of the fitted parameter were greater for the used polyethersulfone membrane, which indicating a more severe fouling during the Humic acids ultrafiltration process.

### References

1. Radwan A, Willey RJ, Davies G, Fataftah A, Ghabbour EA, et al. (1996) Supercritical fluid CO2 extraction accelerates isolation of humic acid from live Pilayella littoralis (Phaeophyta). J Applied Phycology 8: 545-551.
2. Ghabbour EA, Davies G (2001) Humic Substances, Structures, Models and Functions. RSC Advances.
3. Shao J, Hou J, Song H (2011) Comparison of humic acid rejection and flux decline during filtration with negatively charged and uncharged ultrafiltration membranes. Water Research 45: 473-482.
4. Duarte RMBO, Santos EBH, Duarte AC (2003) Spectroscopic characteristics of ultrafiltration fractions of fulvic and humic acids isolated from a eucalyptus bleached Kraft pulp mill effluent. Water Research 37: 4073-4080.
5. Li H, Jin Y, Nie Y (2009) Application of alkaline treatment for sludge decrement and humic acid recovery. Bioresour Technol 100: 6278-6283.
6. Ramunni AU, Palmieri F (1985) Use of ultrasonic treatment for extraction of humic acid with inorganic reagents from soil. Org Geochem 8: 241-246.
7. Adani F, Ricca G (2004) The contribution of alkali soluble (humic acid-like) and unhydrolyzed-alkali soluble (core-humic acid-like) fractions extracted from maize plant to the formation of soil humic acid. Chemosphere 56: 13-22.
8. Cho KT, Lwin MZ (2012) Study on the Analysis of Nitrohumic Acids from Two Different Rank Myanmar Coal by Ultraviolet Spectroscopy, International Conference On Chemical Processes And Environmental Issues (ICCEEI'2012) Singapore. July 15-16.
9. Ghouas H, Haddou B, Kameche M, Derriche Z, Gourdon C (2012) Extraction of humic acid by coacervate: Investigation of direct and back processes. J Hazard Mater 205-206: 171-178.
10. Kliaugaite D, Yasadi K, Euverink G, Bijmans MFM, Racys V (2013) Electrochemical removal and recovery of humic-like substances from wastewater. Sep Purif Technol 108: 37-44.
11. Ghaly AE, Ananthashankar R, Alhattab M, Ramakrishnan VV (2014) Production, Characterization and Treatment of Textile Effluents: A Critical Review. J Chem Eng Process Technol 5: 182.
12. Lone S, Ahmad S A, Kumar V (2015) Modeling and Simulation of a Hybrid Process (Pervaporation+Distillation) using MATLAB. J Chem Eng Process Technol 6: 234.
13. Li H, Li Y, Zou S (2014) Extracting humic acids from digested sludge by alkaline treatment and ultrafiltration. J Mater Cycles Waste Manage 16: 93-100.
14. Das C, Patel P, De S, Dasgupta S (2006) Treatment of Tanning effluent using nanofiltration followed by reverse osmosis. Sep Purif Technol 50: 291-299.
15. Singh V, Das C (2014) Comparison of spiral wound UF membrane performance between turbulent and laminar flow regimes. Desalination 337: 43-51.
16. Singh V, Jain P K, Das C (2013) Performance of spiral wound ultrafiltration membrane module for with and without permeate recycle: Experimental and theoretical consideration. Desalination 322: 94-103.
17. Das A, Paul D, Golder AK, Das C (2015) Separation of Rebaudioside-A from stevia extract: Membrane selection, assessment of permeate quality and fouling behavior in laminar flow regime. Sep Purif Technol 144: 8-15.
18. Vela MCV, Blanco SA, Garcia JL, Rodriguez EB (2008) Analysis of membrane pore blocking models applied to the ultrafiltration of PEG. Sep Purif Technol 62: 789-498.

**Citation:** Saha S, Das C (2015) Analysis of Fouling Characteristics and Flux Decline during Humic Acids Batch Ultrafiltration. J Chem Eng Process Technol 6: 252. doi:10.4172/2157-7048.1000252